Applied Mechanics and Materials Vols. 3-4 (August 2005) pp. 117-124
online at http://www.scientific.net

Experimental and finite element study of welded T-joints

A. Wu[1], B. G. Mellor[2] and S. Syngellakis[3]

School of Engineering Sciences, University of Southampton, Southampton SO17 1BJ, U.K.
[1] A.WU@soton.ac.uk, [2] bgm@soton.ac.uk, [3] ss@soton.ac.uk

Keywords: Welded joints, material characterisation, bending, strain measurement, failure mechanisms, finite element analysis.

Abstract. Suitable testing arrangements are made for assessing the strength of welded T-joint specimens and providing input for the validation of finite element simulations of their behaviour under load. Material characterisation across the various weld areas is carried out through tensile and hardness tests as well as standard metallographic procedures for examining the microstructure. Strain is measured at critical locations identified through initial FEM analysis. Failure mechanisms are monitored, failure loads recorded and linked to the joint material and geometric characteristics. The consistency of FEM predictions with these measurements and observations provide a reasonable degree of confidence that the developed model can yield reliable stress and strain distributions for failure analysis.

Introduction

A reliable structural design of welded structures requires the accurate assessment of the behaviour of the welded connections. Design practice relies on codes, which have been mostly based on empirical studies [1-3]. Although welds are conventionally designed to be statically stronger than the components they connect, in practice, a large number of fracture failures occur in the weld [4]. This explains the need for further research in this area.

This paper focuses on T-joints because of their complex behaviour and their extensive application in engineering structures, such as fillet-welded T-stiffeners in ship building. Experimental investigation of failure in fillet welds has been extensive. Recent studies focused on welded thin-walled members [5] and moment connections in structural frameworks [6, 7]. Early investigations on the failure loads under bending and shear were hampered by the lack of information on the true stress distributions [8]. Such distributions are more complex than usually assumed due to geometric imperfections, residual stresses and strains as well as the geometric complexity of the connection itself. The photoelastic technique provided limited information on strain distributions over the surface of specimens [9]. Approximate models for stresses at critical locations have been assessed through finite element analysis (FEA) [10]. Reliable material input is essential to the accuracy of FEA predictions. It has been established however that the rapid heating and cooling rates experienced by the weldment during the welding process results in considerable variation of material properties across the connection.

A generic FEA model for a T-joint is developed in order to examine in detail the effect of various geometric and material parameters on its behaviour under continuously increasing loading. Modelling and simulations have been based on ANSYS, a general-purpose FEA package. In parallel, physical T-joints were built, suitably instrumented and tested under bending about the longitudinal axis of the weld. Detailed material characterisation was carried out through tensile and hardness tests. The performance of the FEA model was assessed by comparing its predictions with experimental measurements. The most likely failure mechanisms of joints with various geometric characteristics were identified.

Experimental Work

Welding process. Since the weld strength is of primary interest, the fillet welds were sized so that failure would occur in the weld rather than the base metal. Moreover, such weaker fillet welds are

common in stiffener design where a full strength weld is not necessary. A 500 mm-long attachment was joined to a main plate of the same length by two single-pass fillet welds designed to have a leg length of 7 mm. The cross section of the joint with its nominal dimensions is shown in Fig. 1. The plates were welded by the MIG process without any edge preparation. In order to assist the validation of an FEM simulation of the heat transfer problem, the temperature was monitored at a number of key locations through thermocouples, some of them embedded within the joint plates.

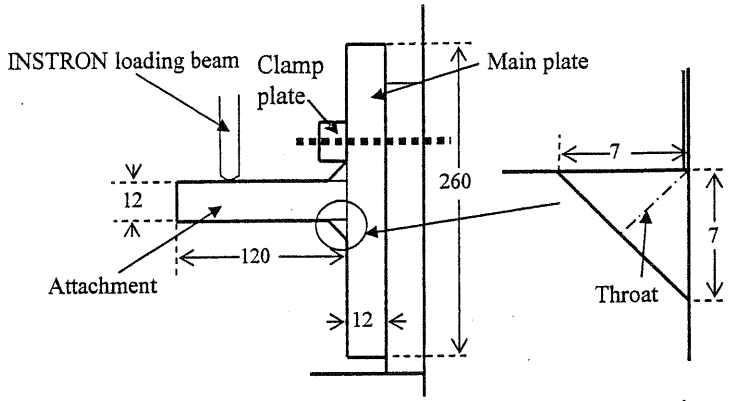

Figure 1. T-joint cross-section with the nominal dimensions of the T1 specimen (in mm)

Micrographs of etched specimens, as that shown in Fig. 2(a), revealed defects in the left, first pass fillet weld. The effect of such defects was assessed through tests and analysis based on this rather imperfect weldment, which was labeled T1. It was however considered important to study, in parallel, the behaviour of welded joints of acceptable quality for engineering applications. A commercially welded T-joint, labeled T2, was thus obtained for that purpose. The nominal cross-sectional dimensions of both plates welded to form T2 were 90 mm × 10 mm. Its attachment plate was given edge preparation resulting in a good quality weld with only slight variation in fillet size and shape along the longitudinal weld direction although the profiles of the two passes were different. An etched T2-specimen is shown in Fig. 2(b).

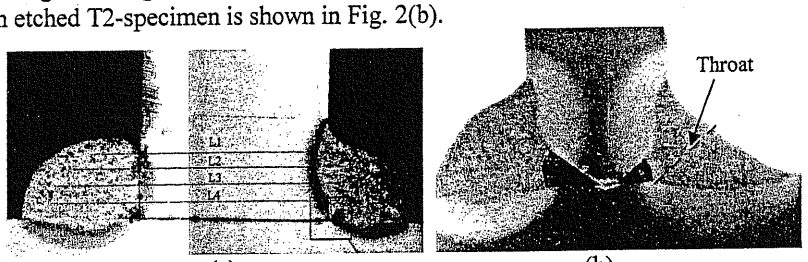

Figure 2. Typical etched specimens (a) T1-weldment, (b) T2-weldment

Material characterisation. Standard tensile tests provided the elasto-plastic stress-strain relations for the base metal of both joints. Round bar tensile specimens were extracted from the weld areas for the same purpose. The results from three tests per joint for the base metal were very consistent. In contrast, greater differences were observed in the results from the two tests for the weld metal. This was attributed to the presence of defects and base metal material in the respective specimens. The values of the yield strength σ_Y, ultimate tensile strength σ_u and elongation to fracture listed in Table 1 are the averages of those obtained from the test records.

Since the heat affected zone (HAZ) is too small to extract a tensile test specimen from it, its mechanical properties were determined by hardness tests. Such a test is not only easily performed and non-destructive but also allows the variation of material properties over an area to be tracked. Simple empirical expressions such as [11, 12]

$$\sigma_Y = \frac{H_v}{3}(0.1)^{m-2} \quad (1)$$

$$\sigma_u = \frac{H_v}{2.9}(3-m)^{3-m}\,[12.5(m-2)]^{m-2} \quad (2)$$

provide the yield and ultimate tensile strength in terms of the Vickers hardness number H_v and the Meyer's index m defined through the relation $W = kd^m$ where W is the Brinell hardness load and d the corresponding indentation diameter.

Table 1 Mechanical properties obtained from tensile tests

Joint	Material	σ_Y [MPa]	σ_u [MPa]	Elongation [%]
T1	Base metal	290	449	25.6
	Weld metal	460	559	10.9
T2	Base metal	658	711	7
	Weld metal	433	539	7

The average Vickers hardness and Meyer's index values obtained from a large number of Vickers and Brinell indentations, respectively, are listed in Table 2. The corresponding values for the yield and ultimate tensile strength, obtained using Eqs. (1) and (2), respectively, are also given in Table 2. For the base metal, the σ_Y estimates are reasonably close to those listed in Table 1, which were directly measured from tensile tests. Regarding σ_u, similar agreement is noted between respective values for T2 but considerable difference in the case of T1. The latter can be attributed to absence of work hardening in the T1 base metal resulting in high m value and hence overestimation of σ_u by Eq. (2). For the weld metal, the results from the hardness tests are considerably higher, especially in the case of T1. This is consistent with the difficulty of producing good quality weld metal tensile test specimens highlighted above. The differences in the material properties of the base metal, weld metal and HAZ were found consistent with the microstructure of these three areas.

Table 2 Mechanical properties obtained from hardness tests

Joint	Material	Vickers hardness	Meyer's index	σ_Y [MPa]	σ_u [MPa]
T1	Base metal	165	2.23	310	567
	Weld metal	230	2.01	718	738
	HAZ	218	2.23	422	767
T2	Base metal	218	2.01	694	712
	Weld metal	176	2.01	558	573
	HAZ	165	2.22	329	581

Bending tests. Six specimens of approximately 12 mm thickness were cut from each of the two weldments and strain gauges attached to their surfaces. The tests were carried out in an Instron 1196 testing machine. Due to size limitations, only one strain gauge could be fitted to a fillet weld area. Its data would be used to assess the accuracy of the respective FEM results so that strain and stress distribution in the weld area could be reliably predicted. Photographs were taken at regular intervals in order to capture crack initiation and growth. The specimens were divided in two groups, each with different orientation relative to the loading, so that both the first and the second pass were subjected to tension.

Finite Element Modelling

It was evident from the etched specimens (see Fig. 2) that the profile and size of the weld fusion zone as well as the HAZ varied along the welding direction and from one weld pass to the other. This variation could explain the failure path differences between tested specimens. For this reason, the actual weld profiles of specific specimens were modelled as accurately as possible. A rigorous modelling of the support system was also adopted in order to account for any additional deflections due to its compliance. The load was simulated through displacement of the loading beam (see Fig. 1). Kinematic strain hardening plasticity was implemented through the multi-linear ANSYS model. The stress-strain curves directly obtained from the tensile tests were used for the base metal. For reasons explained in the characterization section, the stress-strain input for both the weld metal and HAZ was based on the data of Table 2 generated from the hardness tests.

The solid model was meshed with 4-node quadrilateral plane stress elements. Contact elements were introduced on all joint-support/loading interfaces as well as on opposite surfaces of defects. A rational distribution of element sizes ensured that the mesh was sufficiently refined in critical areas, that is, welds and HAZ as well as adjacent to the interface between the loading beam and the attachment plate of the joint. In order to examine the sensitivity of the solution to mesh refinement, the originally adopted element sizes were uniformly reduced by 30% and the results from the respective analyses compared. The maximum von Mises stress difference between the two solutions was only 0.1%.

Temperature records obtained during the welding process contributed to the validation of an earlier FEM analysis for predicting residual stresses [13]. Due to the complexity of a sequential residual-static load stress analysis, a simpler approach was adopted whereby the results from the residual stress analysis were included as initial conditions in the analysis of the joint under static bending load.

Results

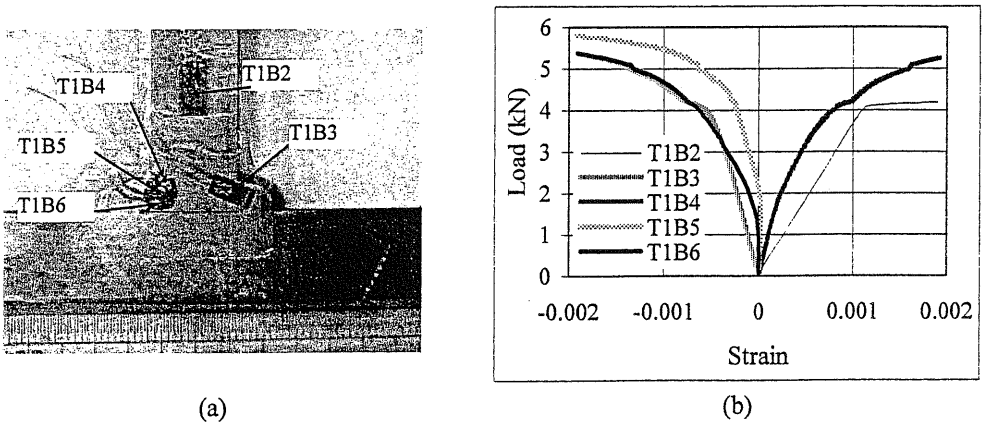

Figure 3 Strain gauge locations in T1B specimen (a) and the corresponding strain records (b).

T1 specimens. The presence of defects was a common feature in all six initially prepared specimens. For this reason only two of them were tested since they were sufficient to demonstrate the significant effect of defects on the strength of the joint. Such defects were mainly attributed to lack of fusion at the weld root. A common failure mode involved early crack propagation initiated by defects leading to eventual coalescence and fracture. The failure loads were only 35%-60% of those predicted by various design codes for defect-free joints of the same size and material properties.

The arrangement of strain gauges on the surface of a specimen from the T1-weldment, labelled T1B, is shown in Fig. 3(a) with the applied load plotted versus the corresponding strain data in Fig. 3(b). The load was applied from left to right so that the first pass on the left was in tension. Unidirectional gauges T1B2 and T1B3 were attached to the base metal of the attachment plate and the HAZ adjacent to the right, second pass, respectively. A rosette composed of gauges T1B4-T1B6 was attached close to the left weld. The high strain and early yield shown by T1B2 can be explained by the presence of defects in the left fillet weld and the weakness of the base relative to weld metal as indicated in Tables 1 and 2. As expected, T1B3 shows compression while the rosette reveals predominantly tension in the direction of T1B4 but also compression in the direction of the other two gauges.

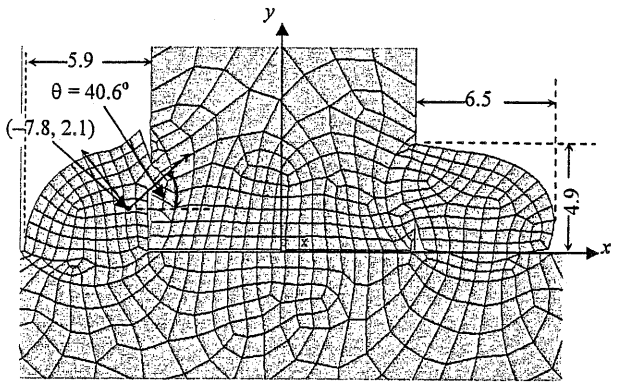

Figure 4 FEM model for the weld area of T1B, dimensions in mm

Fig. 4 shows a detail of the FEM model for T1B with the coordinates of the bottom left corner of the strain gauge rosette on the left fillet weld as well as a local coordinate system for identifying all the nodes lying within the rosette area. This figure gives a clear indication of the extent of defects, which were traced from a scanned micrograph of the etched section. The principal strains were evaluated from the rosette strain data and their dependence on load is shown in Fig. 5, together with that of the corresponding FEM results. For comparison purposes, the latter were obtained from the averages of the FEM nodal strains over the rosette area.

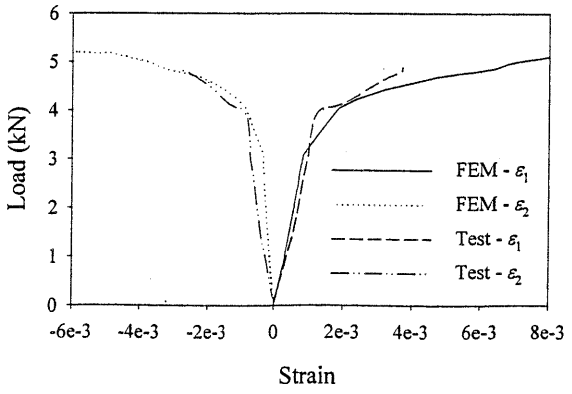

Figure 5 Experimental and predicted principal strains at the rosette in specimen T1B

T2 specimens. Ductile failure was initially observed in all specimens. Yielding first appeared at the weld toe or root and spread with increasing load until cracks were initiated. As the main crack propagates, the load-carrying capacity of the specimen starts to fall.

Several specimens failed in the weld others in the attachment plate. The difference in the respective failure loads was found to be small with those causing weld failure being generally lower. All failure loads were 30-40% higher than those calculated based on design codes confirming the high quality of this weldment.

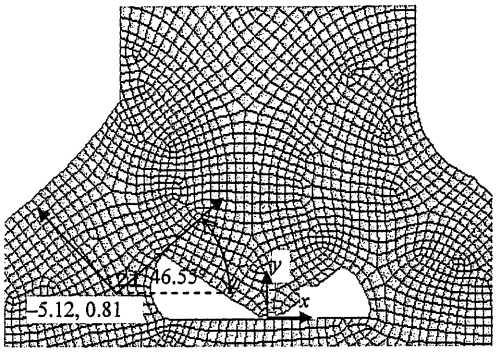

Figure 6 Detail of the T2F FEM model around the weld area

The considerable variation in the strain data obtained from the six specimens indicated their high sensitivity to geometric and material variations in the longitudinal direction. As with the T1 weldment, one particular T2 specimen, designated T2F, was rigorously modelled and analysed. The central part of the model with the position of the strain gauge rosette on the left fillet weld is shown in Fig. 6. The respective experimental and FEA principal strains are shown in Fig. 7. The discrepancy between them illustrates the difficulty of capturing accurately the strain over a small area with a highly non-uniform strain distribution. The residual stresses due to welding, included as initial conditions in FEA, had a rather small effect on the predicted strains.

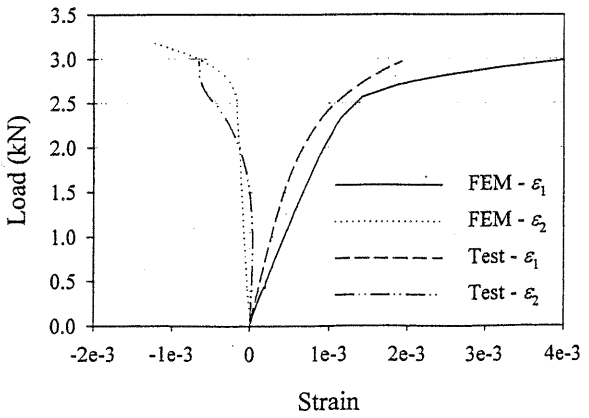

Figure 7 Experimental and predicted principal strains at the rosette in specimen T2F

Discussion

Both tensile and hardness tests indicated that the base metal of T2 had a much higher yield strength than the weld metal. This, combined with the size of the fillet weld, meant that T2 was approximately matched rather than undermatched as originally designed. As the welds were manually made, variations in the weld geometry, microstructure, size of HAZ, presence of defects were inevitable. This explains the difference in failure mode between specimens cut from the same weldment. In common with observations by previous investigators, the failure plane (see Fig. 8) did not coincide with the throat area as assumed by the codes.

Figure 8 Failure mode of T2F specimen

FEM predictions of stress and strain development were examined for various values of critical geometric parameters such as the fillet weld leg length. These results indicated changes in possible failure paths fully corresponding to experimental observations. Similarly, FEM predictions of strain distributions around defects indicated likely locations of fracture paths, which were consistent with actually observed failures. Discrepancies, especially within the elastic deformation range, highlighted the difficulty of measuring accurately the strain within a small area with a highly non-uniform strain distribution. An important drawback in specifying the residual stresses as initial stresses in the static load analysis is the omission of the plastic strains developing during the welding process. The results of such coupled analysis were interpreted taking this limitation into consideration.

Conclusions

A wide range of experimental techniques are required for assessing the performance of a welded T-joint under load. Yet the information they provide cannot be considered complete due to the large variety and uncertainty in the parameters involved and the complexity of the stress and strain fields developed. The under- or over-estimation of failure loads by standard procedures points to the need for refinement of the relevant design formulae. Micro-hardness tests can provide reasonably accurate estimates of varying mechanical properties within small material volumes such as those encountered in weldments. This is essential to the accurate FEM simulation of a welded joint under load. A commercially available FEM package was found suitable for a reliable simulation of a T-joint behaviour under bending load and prediction of its failure loads and mechanisms. Residual stresses due to welding were found to reduce the yield load, they can therefore be associated with failures occurring at low cyclic loads such as fatigue fracture.

The work presented here should be considered as a modest contribution towards the development of a comprehensive analytical tool for predicting failure mechanisms, particularly under fatigue loading. Thus the essential features of the complex FEM models generated could be identified and transferred to relatively simple joint models incorporated within global structural analysis tools.

References

[1] L.J. Butler, S. Pal and G.L. Kulak: J. Struct. Div-Proc. ASCE Vol. 98 (1972), p. 989
[2] B.G. Mellor, R.C.T. Rainey and N.E. Kirk: Mater. Des. Vol. 20 (1999), p. 193
[3] G.S. Miazga and D.J.L. Kennedy: Can. J. Civ. Eng. Vol. 16 (1989), p. 583
[4] T.R. Higgins and F.R. Preece: Welding J. Res. Suppl. Vol. 47 (1968), p. 429s
[5] X.-L. Zhao, R. Al-Mahaidi and K.P. Kiew: J. Struct. Eng. Vol. 125 (1999), p. 821
[6] R.J. Dexter and M.I. Melendrez: J. Struct. Eng. Vol. 126 (2000), p. 24
[7] J.M. Ricles, J.W. Fisher, L.-W. Lu and E.J. Kaufmann: J. Constr. Steel Res. Vol. 58 (2002), p. 565
[8] F.E. Archer, H.K. Fischer and E.M. Kitchen: Civ. Eng. Pub. Works Rev. Vol. 54 (1959), p. 455
[9] H. Fessler and C. Pappalettere: J. Strain Anal. Vol. 24 (1989), p. 15
[10] O. Doerk, W. Fricke and C. Weissenborn: Int. J. Fatigue Vol. 25 (2003), p. 359
[11] J.R. Cahoon, W.H. Broughton and A.R. Kutzak: Metall. Trans. Vol. 2 (1971), p. 1979
[12] D. Tabor: *The Hardness of Metals* (Clarendon Press, Oxford 1951)
[13] A. Wu, S. Syngellakis and B.G. Mellor: *Proc. 6th Int. Conf. on Trends in Welding Research* (ASM Int., 2003), p. 832